ROYAL SOCIETY
OF CHEMISTRY

PAPER
Frank Tambornino *et al.*
Synthesis, XRD and DFT studies on Pb[ChCN]$_2$ (Ch = O, S, Se)
and Pb[SeCN][OH]

Check for updates

Synthesis, XRD and DFT studies on Pb[ChCN]$_2$ (Ch = O, S, Se) and Pb[SeCN][OH]†

Alena Shlyaykher,[a] Aleksandar Živković, [ID] [b,c] Hennes Günther,[a] Anna Lea Barba,[a] Nora H. de Leeuw [ID] [b,d] and Frank Tambornino [ID] *[a]

We report on the synthesis of Pb[ChCN]$_2$ (Ch = O, S, Se) and Pb[SeCN][OH] and their hitherto unknown crystal structures. All products were fully characterized by single-crystal and powder X-ray diffraction. Bulk analysis was performed by Rietveld refinement, elemental analysis, differential scanning calorimetry–thermogravimetric analysis (DSC–TGA), and solid-state Raman spectroscopy. Quantum-mechanical calculations based on the density functional theory allowed optimization of the structural parameters of these lead-based compounds, as well as assessment of their electronic structures and detailed assignment and interpretation of the vibrational spectra. In addition, the origin of bands related to difficulties in assigning the exact position of H atoms in the structures was resolved.

Introduction

Chalcogenocyanates are archetypal pseudohalide anions with the general formula [ChCN]$^-$ (Ch = chalcogen). Four of the six theoretically possible candidates have been synthesized so far: cyanate [OCN]$^-$, thiocyanate [SCN]$^-$, selenocyanate [SeCN]$^-$, and tellurocyanate [TeCN]$^-$. However, only the binary salts of the two lightest homologues have been well researched and feature in introductory and general chemistry textbooks.[1] One of the prominent compounds in the series of cyanates is ammonium cyanate, [NH$_4$][OCN]. Almost 200 years ago Liebig and Wöhler discovered its ability to rearrange into urea, [NH$_2$]$_2$CO, a compound with the same sum formula but different structure. From this finding, they deduced the, at the time, revolutionary concept of isomerism, which has remained essentially unchanged until the present day.[2] However, not only ammonium cyanate, but also a number of quasi-binary metal cyanates show the ability to yield urea, *e.g.*, by heating with water. Lead cyanate, Pb[OCN]$_2$, reacts with two equivalent measures of water to produce urea and lead carbonate, Pb[CO$_3$], which allows the facile synthesis of pure urea. The progress of this reaction can be observed by the transformation of crystalline Pb[OCN]$_2$ to an amorphous solid of lead carbonate Pb

[CO$_3$].[3,4] The first mention of Pb[OCN]$_2$ dates back to the year 1815, when Gay-Lussac combined lead(II/IV) oxide, Pb$_3$O$_4$, with an aqueous solution of cyanogen, [CN]$_2$. The reaction mixture was transformed from a colourless suspension to a lemon-yellow solution, which was observed to react with calcium carbonate to form ammonia.[5] In 1823, Wöhler synthesized Pb[OCN]$_2$ from aqueous solutions of lead acetate and a cyanate and isolated the product as a white, light-polarising, crystalline precipitate, which was only slightly soluble in water, but soluble in ammonia.[3,6] However, the only reported analytical data for Pb[OCN]$_2$ was the elemental analysis of lead performed by precipitating it as lead sulphate.

In the past, a compound erroneously identified as Pb[SCN]$_2$ was synthesized by Liebig[7] by adding a neutral solution of lead salt to a moderately concentrated solution of an alkali metal thiocyanate. The product was obtained in the form of white to faintly yellow anhydrous crystals, which were only sparingly (about 1%) soluble in cold water. As was known for several (pseudo-)halide salts, Pb[SCN]$_2$ was slightly more soluble in solutions of thiocyanates.[8] In addition, it was mentioned that Pb[SCN]$_2$ synthesized from lead acetate was sensitive towards light and turned dark. It was found later that synthesis in a neutral medium delivered a mixture of lead thiocyanate, Pb[SCN]$_2$, and basic lead thiocyanate, Pb[SCN][OH]. The crystal structure of Pb[SCN]$_2$ was determined in 1966,[9] followed in 1995 by a revised and more accurate model.[9,10] Pure lead thiocyanate hydroxide, Pb[SCN][OH], can also be obtained by boiling crystals of Pb[SCN]$_2$ in water, or by precipitating an aqueous thiocyanate solution with basic lead acetate, the latter leading to a white curd-like precipitate. By combining with lead halide salts, Pb[SCN]$_2$ is converted to a number of "double salts", *e.g.* water-soluble Pb[SCN]$_2$·PbCl$_2$, Pb[SCN]$_2$·PbI$_2$, and Pb[SCN]Cl, or the less soluble Pb[SCN]$_2$·8 PbBr$_2$.[8]

[a]*Philipps-Universität Marburg, Hans-Meerwein Straße 4, Marburg, DE-35032, Germany. E-mail: frank.tambornino@chemie.uni-marburg.de*
[b]*Department of Earth Sciences, Utrecht University, 3548CB Utrecht, The Netherlands*
[c]*Institute of Inorganic Chemistry, Christian-Albrecht University of Kiel, 24118 Kiel, Germany*
[d]*School of Chemistry, University of Leeds, Leeds LS2 9JT, UK*

Recently, $Pb[SCN]_2$ has found application as a material for photovoltaic elements. For example, $(CH_3NH_3)_2Pb(SCN)_2I_2$ was synthesized by halide substitution starting from $CH_3NH_3PbI_3$ and it was shown to be a promising candidate for lower-dimensional hybrid-halide compounds.[11] Other reports demonstrated that materials with the pseudo-halide $[SCN]^-$ show higher moisture tolerance, device stability in solar cells, and reduced trap-assisted recombination.[12–15]

The synthesis of the heaviest compound in the series, lead selenocyanate, $Pb[SeCN]_2$, was reported as early as 1851.[16] The product was obtained as "lemon-yellow" needles by precipitation from a boiling acidic suspension of lead oxide with an aqueous solution of $K[SeCN]$ and subsequent recrystallization. $Pb[SeCN]_2$ was solely analysed by elemental analysis and described as insoluble in alcohol and thermally stable up to 100 °C. Further analytical data were not reported.[16]

Here, we report on the synthesis of $Pb[OCN]_2$, $Pb[SeCN]_2$ and $Pb[SeCN][OH]$, as well as their hitherto unknown crystal structures, properties obtained from solid-state density functional theory calculations, vibrational spectra and thermal behaviour. In this context, the crystal structure and properties of the related $Pb[SCN]_2$ are revisited.

Experimental section

General synthetic methods

All reactions and operations were performed in air. Lead acetate trihydrate (university stocks, purity confirmed by PXRD), potassium hydroxide (85.0%, Chemsolute), potassium cyanate (97%, Merck), potassium thiocyanate (university stocks, purity confirmed by PXRD), deuterium oxide (99.9%, www.deutero.de), and acetic acid (99–100%, GPR Rectapur) were obtained from commercial sources. Potassium selenocyanate was prepared following the literature procedure.[1] Sodium deuteroxide was prepared following the literature procedure.[17]

Preparation of $Pb[OCN]_2$ following a modified procedure by Wöhler.[6] $Pb[CH_3COO]_2·3 H_2O$ (702 mg, 1.85 mmol, 1.0 eq.) and $K[OCN]$ (300 mg, 3.70 mmol, 2.0 eq.) were each dissolved in 20 mL of distilled H_2O, respectively. The solution of $Pb[CH_3COO]_2$ was cooled to 0 °C and 1 mL of concentrated acetic acid was added. Both solutions were combined, and a colourless precipitate was formed slowly. After 30 minutes, the suspension was filtered through a 2 μm paper filter, washed with 50 mL of acetone, 30 mL of diethyl ether and dried in air. The product (151 mg, 0.52 mmol) was obtained as a colourless crystalline powder in 28% yield, already containing single crystals suitable for X-ray diffraction. Elemental analysis (%): calcd for $Pb[OCN]_2$: C, 8.25; N, 9.62. Found: C, 8.49; N, 9.53.

Preparation of $Pb[SCN]_2$ following a modified procedure by Woodward.[8,9] $Pb[CH_3COO]_2·3 H_2O$ (200 mg, 0.527 mmol, 1.0 eq.) and $K[SCN]$ (102 mg, 1.054 mmol, 2.0 eq.) were each dissolved in 20 mL of distilled H_2O, respectively, and cooled to 0 °C in an ice bath. To the solution of $K[SCN]$, 1 mL of concentrated acetic acid was added. Both solutions were combined, and a colourless precipitate was formed. The suspension was filtered through a 2 μm

paper filter, washed with 50 mL of water and dried in air. The product (95 mg, 0.29 mmol) was obtained as a colourless crystalline powder in 56% yield. Crystals suitable for X-ray diffraction were grown by layering an acidic aqueous solution (acidified with acetic acid) of lead acetate with an aqueous solution of potassium thiocyanate. Elemental analysis (%): calcd for $Pb[SCN]_2$: C, 7.43; N, 8.66; S, 19.83. Found: C, 7.77; N, 8.66; S, 20.08.

Preparation of $Pb[SeCN]_2$ following a modified procedure by Crookes.[16] $Pb[CH_3COO]_2·3 H_2O$ (500 mg, 1.32 mmol, 1.0 eq.) and $K[SeCN]$ (418 mg, 2.90 mmol, 2.2 eq.) were each dissolved in 20 mL of distilled H_2O, respectively. To the solution of $Pb[CH_3COO]_2$, 1 mL of concentrated acetic acid was added. Both solutions were combined, and a yellowish precipitate was formed immediately. The suspension was filtered through a 2 μm paper filter, washed with 50 mL of water and dried in air. The product (395 mg, 0.94 mmol) was obtained as a yellowish crystalline powder in 72% yield. Crystals suitable for X-ray diffraction were grown by layering an acidic aqueous solution (acidified with acetic acid) of lead acetate with an aqueous solution of potassium selenocyanate. Elemental analysis (%): calcd for $Pb[SeCN]_2$: C, 6.72; N, 5.76. Found: C, 6.51; N, 6.25.

Preparation of $Pb[SeCN][OH]$. $Pb[CH_3COO]_2·3 H_2O$ (541 mg, 1.43 mmol, 1.0 eq.), $K[SeCN]$ (206 mg, 1.43 mmol, 1.0 eq.) and $K[OH]$ (80 mg, 1.43 mmol, 1.0 eq.) were dissolved in 10 mL of distilled H_2O, respectively. The solution of $K[OH]$ was then added to the solution of $K[SeCN]$. Next, the resulting solution was combined with the solution of $Pb[CH_3COO]_2$. A colourless powder was precipitated immediately. The suspension was filtered through a 2 μm paper filter, washed with 50 mL of water and dried in air. The product (267 mg, 0.81 mmol) was obtained as a colourless crystalline powder in 57% yield. Crystals suitable for X-ray diffraction were grown by layering an aqueous solution mixture of lead acetate and potassium hydroxide with an aqueous solution of potassium selenocyanate. Elemental analysis (%): calcd. For $Pb[SeCN][OH]$: C, 3.65; N, 4.25; H, 0.31. Found: C, 4.03; N, 4.24, H, 0.04.

Preparation of $Pb[SeCN][OD]$. $Pb[CH_3COO]_2·3 H_2O$ (997 mg, 2.63 mmol, 1.0 eq.) and $K[SeCN]$ (374 mg, 2.63 mmol, 1.0 eq.) were dissolved in 15 mL of D_2O, respectively. The solution of $K[SeCN]$ was combined with the solution of $Na[OD]$ (108 mg, 2.63 mmol, 1.0 eq.) in 20 mL of D_2O and allowed to cool to 0 °C in an ice bath. Next, the resulting solution was precipitated with the solution of $Pb[CH_3COO]_2$. The obtained colourless suspension was filtered through a 2 μm paper filter, washed with 50 mL of D_2O, 30 mL of acetone, and dried in air. $Pb[SeCN][OD]$ was obtained as a colourless crystalline powder in 58% yield (502 mg, 1.52 mmol). Elemental analysis (%): calcd. for $Pb[SeCN][OD]$: C, 3.64; N, 4.24; H, 0.61. Found: C, 4.04; N, 3.79, H, 0.05.

Methods

Single-crystal X-ray structure determination

Single-crystal X-ray diffraction data were collected using an IPDS-2 (STOE, Darmstadt) diffraction system equipped with a source of mirror-monochromated Mo Kα radiation

(λ = 0.7107 Å, Xenocs Microfocus Source) and an Image Plate detector. Crystals were selected under Paratone-N oil, mounted on micromount loops, and quench-cooled using an Oxford Cryosystems open-flow N_2 cooling device. Data were collected at 100 K or 180 K and processed using the X-Area program package, including unit-cell parameter refinement and interframe scaling (which was carried out using LANA within X-Area).[18] The structure was subsequently solved using direct dual-space methods (SHELXT[19]) and refined on F^2 with SHELXL using the Olex2[20] user interface. The crystal structure drawings were generated with DIAMOND.[21]

Powder X-ray diffraction

Powder X-ray diffraction patterns were recorded on a STADI MP (STOE, Darmstadt) powder diffraction system equipped with a source of mirror-monochromatized Cu-Kα1 radiation (λ = 1.54175 Å) and a silicon-strip MYTHEN 1K detector. Data were collected at room temperature in transmission mode (Debye–Scherrer geometry). The powder samples were ground in agate mortars and flame-sealed in glass capillaries (inner diameter: 0.3 mm, Hilgenberg, Malsberg, Germany). For additional details, see Table S3.† Subsequent Rietveld refinements[22] were performed with the TOPAS 7.0 program package.[23] The structural models derived from single-crystal X-ray data were used as starting points for the refinements. Background functions were modelled using shifted Chebyshev polynomials, and profile functions were described with the modified Thompson–Cox–Hastings pseudo-Voigt "TCHZ" function as implemented in TOPAS. For additional details, see Table S3.† High-temperature powder X-ray diffraction patterns were recorded on a STADI P (STOE, Darmstadt) powder diffraction system equipped with a source of mirror-monochromatized Ag-Kα1 radiation (λ = 0.55941 Å) and a silicon-strip MYTHEN 1K detector. Data were collected in transmission mode (Debye–Scherrer geometry).

Quantum-mechanical calculations

Density functional theory (DFT) calculations were performed using the all-electron code CRYSTAL.[24–27] The global hybrid B3LYP exchange-correlation functional was used throughout the work[28,29] (unless stated otherwise) together with the Peintinger–Oliveira–Bredow triple-ζ-valence + polarization basis set (pob-TZVP rev2).[30] For Pb, an effective core potential was used. The Coulomb and exchange series were summed directly and truncated using overlap criteria with thresholds of 10^{-7}, 10^{-7}, 10^{-7}, 10^{-7}, and 10^{-14}, as described previously.[31,32] Reciprocal space[33] was sampled according to a shrinking factor (input IS) of (3 7 3) for bulk Pb[SeCN]$_2$ and Pb[SeCN][OH] and (7 7 3) for Pb[SCN]$_2$ and Pb[OCN]$_2$. Long-range dispersion corrections were included using the semiempirical D3 approach of Grimme *et al.* with Becke–Johnson damping.[34–36] Band structure calculations were performed on optimized geometries along high-symmetry directions obtained using the SeeK-path interface.[37]

Infrared and Raman intensities were calculated analytically through the coupled-perturbed/Kohn–Sham approach for the harmonic vibrational analysis.[38,39] Integrated Raman intensi-

ties were normalised so that the most intense peak was set to 1000. The peak width is not explicitly available within this treatment; thus, it was kept constant. The spectra were constructed by using the transverse optical modes and adopting a pseudo-Voigt function with the default VOIGT and DAMPFAC variables of 1.0 (pure Lorentzian functions) and 8.0 (full width at half maximum used for the spectra), respectively. The temperature and laser wavelength, considered through a prefactor in the expression for the Raman integrated intensity, were set to 295 K and either 532 nm or 633 nm to facilitate comparison with experimental measurements.

Anharmonicity was treated using two different approaches. In the first approach, anharmonic effects were taken into account only for the O–H stretching mode by numerically solving the one-dimensional Schrödinger equation.[40,41] In the second approach, anharmonic vibrational states were computed by solving the vibrational self-consistent field (VSCF) equations (where each mode interacts with an average potential of all the other modes) and the vibrational configuration interaction (VCI) equations, which allow for explicit mode–mode coupling treatment.[42,43] The Energy–Gradient–Hessian (EGH) two-point finite difference scheme was used to compute high-order energy derivatives with a displacement of 0.9 in terms of the classical amplitude of each normal mode.[44] By exploiting point symmetry, the number of distinct atomically displaced nuclear configurations that need to be explored for energy and force calculations is significantly reduced and made computationally tractable.[45]

Vibrational spectroscopy

Raman spectra were recorded on a MonoVista CRS + confocal Raman microscope (Spectroscopy & Imaging GmbH) using a 532 nm or 633 nm solid-state laser and a 300 grooves per mm grating. Samples were sealed in borosilicate ampoules at room temperature. Post-acquisition treatment of Raman spectra was achieved with the Origin[46] program package.

Thermogravimetric analysis/differential scanning calorimetry (TGA/DSC) measurements

TGA/DSC measurements were performed by in-house service personnel under a nominally dry nitrogen atmosphere in an MBraun UNIlab glovebox using a DSC-TGA 3 (Mettler Toledo) device. Post-acquisition treatment of the data was performed with the Origin[46] program package.

Elemental Analysis

Elemental analyses were performed by the in-house service personnel. CHN analyses were performed on a CHNS(S)-Analysator Vario MICRO CUBE (Elementar).

UV-vis spectroscopy

Optical absorption spectra were collected on a Varian Cary 5000 UV/Vis/NIR spectrometer in the range of 200–800 nm in diffuse reflectance mode employing a Praying Mantis accessory (Harrick) with automatic baseline correction. Ba[SO$_4$] was used as the white standard. To dilute the sample and reduce artefacts, the compounds were ground together with Ba[SO$_4$] (10%

of the studied compound by weight). The raw data were transformed from reflectance R to absorption according to the Kubelka–Munk function ($F(R) = (1 − R)^2/2R$).

Results and discussion

$Pb[OCN]_2$ and $Pb[SeCN]_2$ crystallize in the orthorhombic space group *Pnma* (No. 62). However, they do not crystallize as isotypical structures and, surprisingly, neither compound crystallizes as an isotypical structure with their sulfur analogue $Pb[SCN]_2$ (*C2/c*, No. 15).[47]

Synthesis and crystal structure of $Pb[OCN]_2$

$Pb[OCN]_2$ was synthesized by combining an aqueous solution of $K[OCN]$ with an aqueous solution of $Pb[CH_3COO]_2$. Colourless needles, suitable for SC-XRD, precipitated slowly. Afterwards, the product was filtered, washed with acetone and diethyl ether, and dried in air. In contrast to $Pb[SCN]_2$ and $Pb[SeCN]_2$, lead cyanate does not form the hydroxide $Pb[OCN][OH]$ either in neutral or basic environments.

At 100 K, $Pb[OCN]_2$ crystallizes in the orthorhombic space group *Pnma* (No. 62) ($a = 8.569(2)$, $b = 3.9410(9)$, $c = 11.660(3)$ Å) with four formula units in the unit cell, one crystallographically independent Pb site and two independent $[OCN]^−$ anions (Fig. 1; for additional data see Table S4†). All atoms in the unit cell occupy the Wyckoff position 4*c* (.*m*.).

The Pb cation is coordinated by a total number of nine atoms with CN_{Pb} = 6 + 3 in the form of tricapped trigonal prisms with a continuous symmetry measure (csm) of 1.9400.[48] The csm quantifies the minimal distance of movement that the points of an object have to undergo in order to transform into a shape of the desired symmetry (perfect polyhedra strive for csm = 0 and the maximum value of distortion strives for infinity).[48,49] The trigonal prism is built of four N and two O atoms of altogether six cyanate anions (CN "6", Fig. 2, left). Pb–N and Pb–O distances are within the expected range for the sum of their ionic radii ($d_{(Pb–N)} = 2.589(9)–2.685(8)$ Å, $d_{(Pb–O)} = 2.827(8)$ Å).[50] Both faces of the prism, which are built from two N and two O atoms, are capped by O atoms of

Fig. 2 Excerpt of the crystal structure of $Pb[OCN]_2$. Left: coordination polyhedron around Pb. Right: double-chain of polyhedra around Pb extending along [010]. Green: Pb, white: C, blue: N, red: O.

adjacent cyanate anions, respectively ($d_{(Pb–O)} = 2.895(10)$ and $3.173(11)$ Å, CN "+2"). The face of the prism built from four N atoms is capped by an N atom of an additional cyanate anion ($d_{(Pb–O)} = 2.607(13)$ Å, CN "+1"). Both crystallographically independent $[OCN]^−$ anions are almost linear with $∢O–C–N = 176.8(16)$ and $178.8(18)°$, respectively. Along [010] the polyhedra are interconnected *via* common O–N–N faces (basal planes of the trigonal prism) thus forming chains. The chains are connected to each other *via* common N–N edges thus forming "double-chains" (Fig. 2, right).

Within (101), the double-chains are connected *via* common $[OCN]^−$ anions (6× by O-terminus, 4× by N-terminus) as well as common O atoms of the $[OCN]^−$ anions (Fig. 3). Within the *ac*-plane the double-chains form the motif of a monoclinic/oblique rod packing (orange), which in this case is a distorted variant of the hexagonal rod packing (blue).

Phase purity was checked with PXRD and Rietveld refinement, which corroborated the model within close error margins (Fig. 4 and Table S3†).

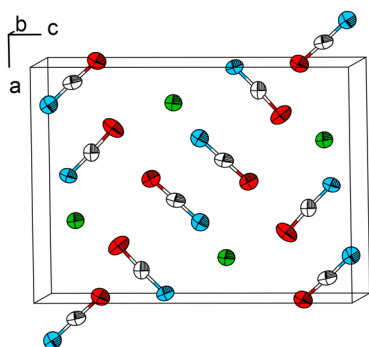**Fig. 1** The crystal structure of $Pb[OCN]_2$. Thermal displacement ellipsoids are drawn at the 75% probability level at 100 K. Green: Pb, white: C, blue: N, red: O.
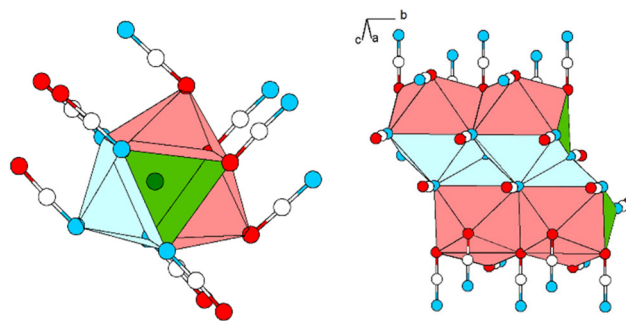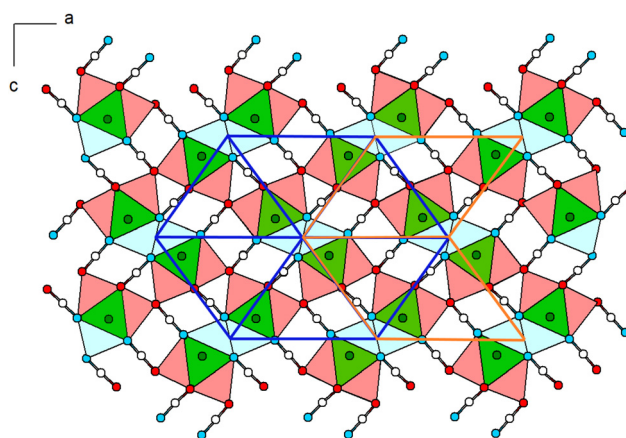

Fig. 3 Extended crystal structure of $Pb[OCN]_2$ viewed along [010]: coordination polyhedra around Pb (green, capped by O in red and N in blue) are connected *via* common $[OCN]^−$ anions and O atoms. The polyhedra form a monoclinic packing (outlined in orange), which can be interpreted as a distorted hexagonal rod packing (blue). Green: Pb, white: C, blue: N, red: O.
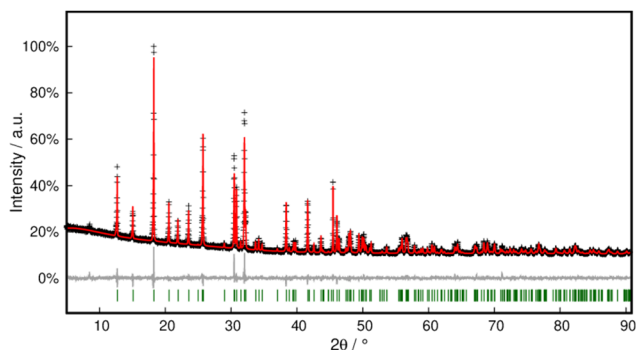
Fig. 4 Rietveld refinement of Pb[OCN]$_2$ at 298 K. Black crosses display measured data; the red line represents the refined model, green bars indicate Bragg positions and the grey line displays the difference plot. Further data are compiled in Table S3.†

Synthesis and crystal structure of Pb[SCN]$_2$

Pb[SCN]$_2$ was synthesized *via* a modification of the literature procedure.[7] To an aqueous solution of K[SCN], a small amount of concentrated acetic acid was added. Upon combining this solution with an aqueous solution of Pb[CH$_3$COO]$_2$, a colourless solid was precipitated immediately, which was washed with distilled water and dried in air. Single crystals of Pb[SCN]$_2$ in the form of slightly yellow needles were obtained by layering a solution of Pb[CH$_3$COO]$_2$ with an aqueous and slightly acidified solution of K[SCN].

At 100 K, Pb[SCN]$_2$ crystallizes in the monoclinic space group $C2/c$ (No. 15) (a = 9.6128(9), b = 6.5306(6), c = 8.1913(7) Å, β = 92.734(7)°), (*cf.* Mokuolu & Speakman: a = 9.661(4), b = 6.544(3), c = 8.253(3) Å, β = 92.37(2)° ref. 47) with four formula units in the unit cell, one crystallographically independent Pb site and one independent [SCN]$^-$ anion (Fig. 5; for additional data see Table S4†). Here, the Pb atom occupies the Wyckoff position 4e (2), while the atoms of the [SCN]$^-$ anion lie in the Wyckoff position 8f (1).

In Pb[SCN]$_2$ the Pb atom lies on a two-fold rotation axis and is surrounded by four N ($d_{(Pb-N)}$ = 2.6820(3), 2.766(3) Å) and

four S ($d_{(Pb-S)}$ = 2.9862(2), 3.1180(7) Å) atoms from eight [SCN]$^-$ units, forming a distorted tetragonal antiprism with a continuous symmetry measure (csm) of 0.7598 (Fig. 6, left). The basal planes of the antiprism are constructed by two N and two S atoms of four [SCN]$^-$ anions, respectively. The [SCN]$^-$ anions are surrounded by four Pb atoms in total: two are adjacent to the N terminus and two Pb atoms are adjacent to the S terminus, respectively. Alternatively, the coordination sphere can be described as a distorted hetero-disphenoid of four Pb atoms with the C atom as the center of the polyhedron (csm = 0.855249, Fig. 6, right).[48]

The antiprisms around Pb are connected to each other *via* two bridging [SCN]$^-$ anions along [010] and four common S-vertices within the *ab*-plane forming layers within [110] (Fig. 7, left). These layers are stacked along [001] in an ABAB motif, and are connected with each other by sharing common N,N-edges of individual polyhedra (Fig. 7, right).

Synthesis and crystal structure of Pb[SeCN]$_2$

In the past, Pb[SeCN]$_2$ has been reported to be synthesized by precipitation from a selenocyanate solution with lead acetate. After filtration of the suspension and crystallisation, lemon-yellow needles of the product were obtained. The salt was in-
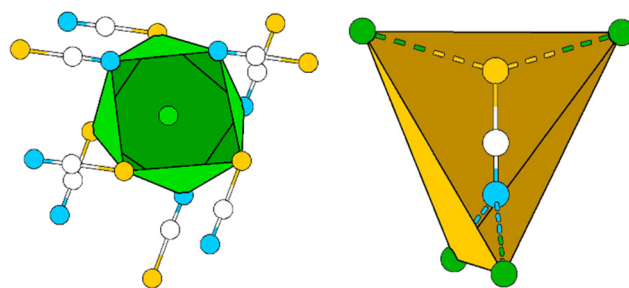

Fig. 6 Excerpt of the crystal structure of Pb[SCN]$_2$. Left: distorted tetragonal antiprism around Pb (green). Right: distorted heterodisphenoid around [SCN]$^-$ (yellow). Green: Pb, white: C, blue: N, yellow: S.
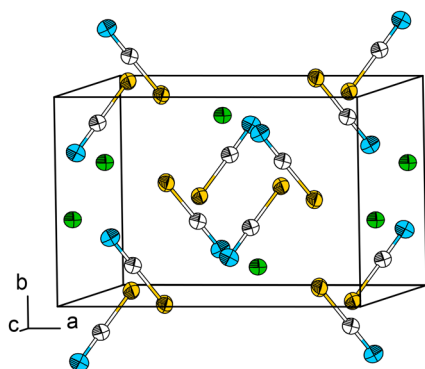

Fig. 5 The crystal structure of Pb[SCN]$_2$. Thermal displacement ellipsoids are drawn at the 50% probability level at 100 K. Green: Pb, white: C, blue: N, yellow: S.
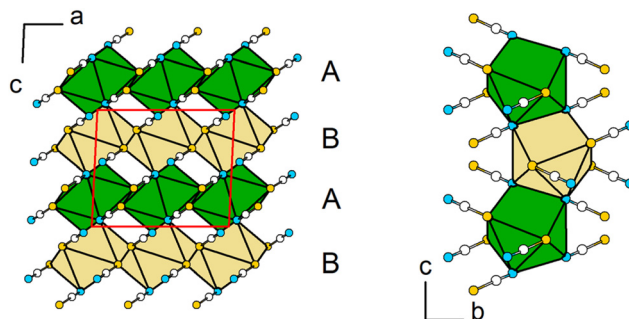

Fig. 7 Extended crystal structure views of Pb[SCN]$_2$ emphasizing the stacking of the coordination polyhedra around Pb. Left: view along [010] with layers of antiprisms around Pb atoms forming an ABAB motif stack along [001]. Right: view along [100], emphasizing the common N,N-edges of the polyhedra. Green: Pb, white: C, blue: N, yellow: S.

soluble in alcohol, and stayed unchanged when heated to 100 °C.[16] Akin to the synthesis of Pb[SCN]$_2$, we repeated the described synthesis but were only able to obtain a mixture of Pb[SeCN]$_2$ and Pb[SeCN][OH]. Pure Pb[SeCN]$_2$ was synthesized by the modification of the literature procedure. To an aqueous solution of K[SeCN], a small amount of concentrated acetic acid was added. Upon combining this solution with an aqueous solution of Pb[CH$_3$COO]$_2$, the product precipitated immediately in the form of yellowish needles suitable for SC-XRD in 72% yield. It was filtered, washed with plenty of water to remove byproducts and subsequently dried under reduced pressure.

At 100 K, Pb[SeCN]$_2$ crystallizes in the orthorhombic space group *Pnma* (No. 62) (*a* = 12.479(2), *b* = 4.2277(9), *c* = 10.6523 (17) Å) with four formula units in the unit cell, one crystallographically independent Pb site and two independent [SeCN]$^-$ anions (Fig. 8; for additional data see Table S4†). In Pb[SeCN]$_2$, as well as in Pb[OCN]$_2$, all atoms occupy the Wyckoff position 4*c* (.*m*.).

The Pb cation is surrounded by a total number of 6 + 1 + 1 atoms in the form of a bicapped trigonal prism (csm = 3.5524). Here, two N and four Se atoms of six selenocyanate anions form a distorted trigonal antiprism (CN "6", Fig. 9, left). Pb–N and Pb–Se distances are within the expected range for the sum of their ionic radii ($d_{(Pb-N)}$ = 3.016(6) Å, $d_{(Pb-Se)}$ = 3.0349(7), 3.1459(8) Å). The face of the prism constructed from four Se atoms is capped by an N atom of an additional selenocyanate unit ($d_{(Pb-N)}$ = 2.419(8) Å, CN "+1"). The *N*,*N*,*Se*,*Se*-face is capped by a Se atom of an additional cyanate anion ($d_{(Pb-Se)}$ = 3.2971(10) Å, CN "+1"). Along [010] the polyhedra are connected by common *N*,*Se*,*Se*-faces (basal planes) to each other, thereby forming chains. The chains are connected to each other *via* common *Se*-vertices to the zig-zag layers within [010] (Fig. 10).

Single layers are connected *via* common almost linear [SeCN]$^-$ anions (∡$_{Se-C-N}$ = 177.6(9), 178.8(8)°), which run along [100] (Fig. 10).

Fig. 9 Excerpts of the crystal structure of Pb[SeCN]$_2$. Left: coordination polyhedron around Pb. Right: double-chain of polyhedra around Pb along [010]. Green: Pb, white: C, blue: N, magenta: Se.

Fig. 10 View of the crystal structure of Pb[SeCN]$_2$ along [010]. Coordination polyhedra around Pb atoms are connected *via* common [SeCN]$^-$ units. Green: Pb, white: C, blue: N, magenta: Se.

Phase purity was checked with PXRD, and Rietveld refinement corroborated the model within close error margins (Fig. 11 and Table S3†).

For the three compounds discussed above, no trends for coordination polyhedra around the central Pb atoms were observed. Whereas in Pb[OCN]$_2$, the Pb atom is surrounded by CN "6 + 3" atoms as a triple-capped trigonal antiprism, the Pb atom in Pb[SCN]$_2$ shows a coordination of eight atoms as a tetragonal antiprism. In Pb[SeCN]$_2$, the Pb atom is surrounded by 6 + 2 atoms as a bicapped trigonal prism. In Fig. 12, the shortest Pb–N und Pb–Ch distances of Pb[ChCN]$_2$ are shown (Ch = O, S, Se). With the increase in the ionic radius of the chalcogen atom, both distances, Pb–N and Pb–Ch, increase, probably due to the increased space needed by the chalcogen atoms that coordinate the Pb atoms. In particular, the change in the Pb–N distance is noticeable.

Furthermore, in the case of capped trigonal prisms in Pb [OCN]$_2$ and Pb[SeCN]$_2$, both are connected to each other by sharing common basal planes, forming rods. These rods are then connected by common edges of polyhedra to the double-chains. In Pb[SCN]$_2$, a completely different motif was observed. Tetragonal antiprisms around Pb are connected by shared vertices and [SCN]$^-$ anions, forming layers. In conclusion, aside from the increase in the Pb–N and Pb–Ch interatomic dis-
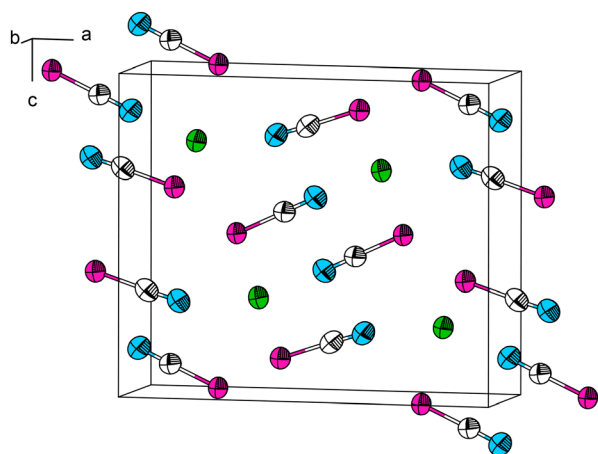

Fig. 8 The crystal structure of Pb[SeCN]$_2$. Thermal ellipsoids are drawn at the 90% probability level at 100 K. Green: Pb, white: C, blue: N, magenta: Se.
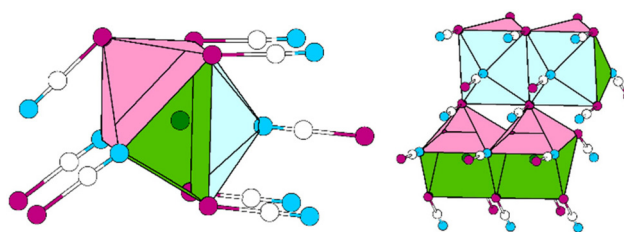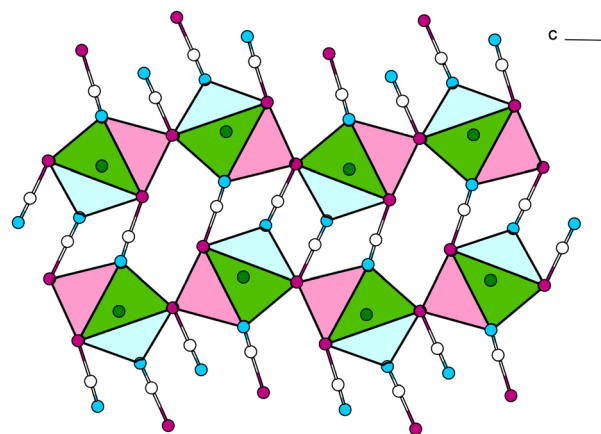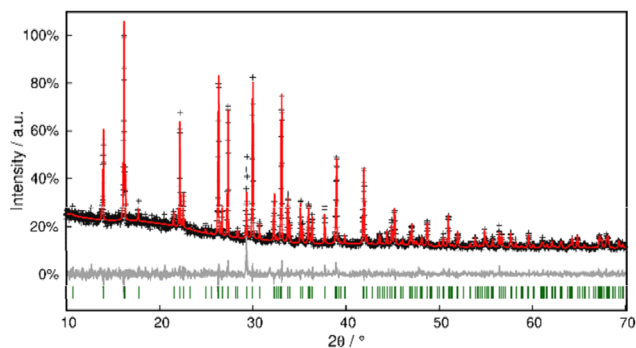
Fig. 11 Rietveld refinement of Pb[SeCN]$_2$ at 298 K. Black crosses display measured data; the red line represents the refined model, green bars indicate Bragg positions and the grey line displays the difference plot. Further data are compiled in Table S3.†
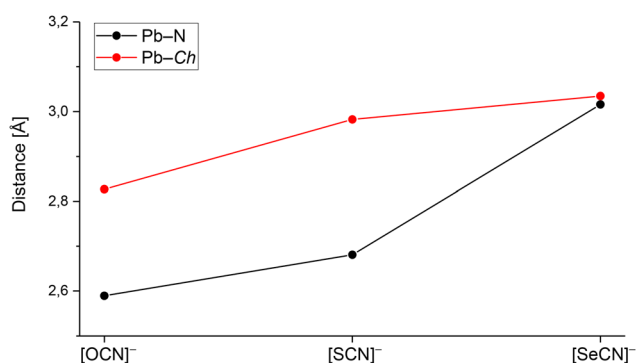

Fig. 12 Pb–N and Pb–Ch distances in Pb[ChCN]$_2$ (Ch = O, S, Se). For each salt the shortest distance was chosen.

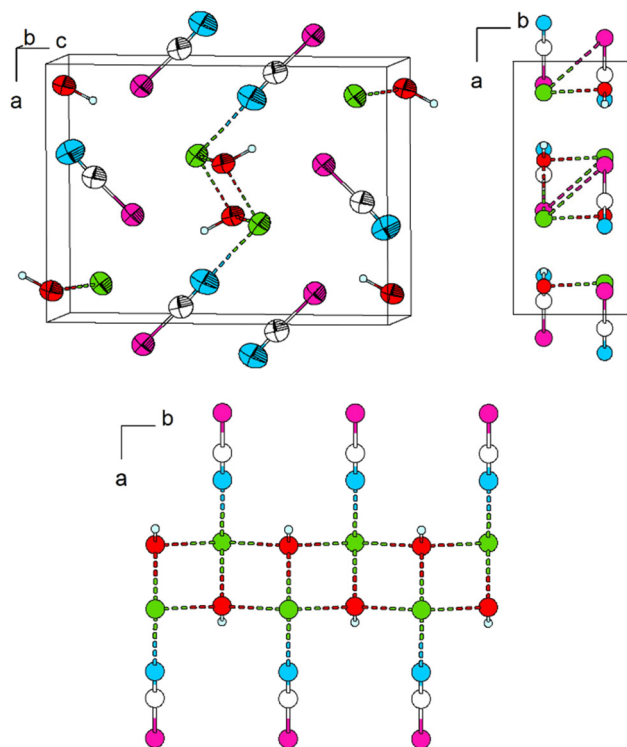**Fig. 13** The crystal structure of Pb[SeCN][OH]. Top left: view of the unit cell approximately along [010]. Top right: view of the unit cell along [001]. Bottom: double-chain of Pb-[OH] units, which runs along [010]. Green: Pb, white: C, blue: N, magenta: Se, red: O, light blue: H. Thermal ellipsoids are drawn at the 90% probability level at 180 K, and hydrogen atoms are drawn with an arbitrary radius.

tances, there are no clear trends visible. The bonding between Pb and the respective anions is ionic in nature and the different packing motifs likely affected by the size of the Ch atom.

Synthesis and crystal structure of Pb[SeCN][OH]

Impure basic lead selenocyanate, Pb[SeCN][OH], mixed with Pb[SeCN]$_2$, can be obtained from the reaction of Pb[CH$_3$COO]$_2$ and K[SeCN]. Pure Pb[SeCN][OH] was obtained by adding an aqueous solution of K[SeCN] to an equimolar aqueous solution of Pb[CH$_3$COO]$_2$ and K[OH]. The product precipitates immediately in the form of a crystalline colourless solid. It was filtered, washed with excess water to remove K[CH$_3$COO], and dried in air. Single crystals in the form of colourless needles were obtained by layering solutions of Pb[CH$_3$COO]$_2$/K[OH] in water with an aqueous solution of K[SeCN].

At 180 K, Pb[SeCN][OH] crystallizes isotypically with Pb[SCN][OH] in the orthorhombic space group *Pnma* (No. 62) (a = 8.6244(2), b = 4.1674(4), c = 11.5412(6) Å) with four formula units in the unit cell (Fig. 13; for additional data see Table S4†). All atoms occupy Wyckoff position 4c (.m.). However, the crystal structure of Pb[SCN][OH] was previously

described as *Pnmb*, a non-standard setting of *Pnma*. The relevant transformation matrix is $\left\{ \begin{matrix} 001 \\ 100 \\ 010 \end{matrix} \right\}$.[10]

For Pb[SeCN][OH], we were not able to determine the positions of the H atoms by single-crystal X-ray diffraction. For structure refinements, restraints were applied in accordance with the chosen space group symmetry. These results were corroborated by solid-state DFT analysis. The presence of the OH group was additionally evidenced by Raman spectroscopy.

In Pb[SeCN][OH], as well as in Pb[SCN][OH], the atoms lie on the mirror plane parallel to [001] at $b = \frac{3}{4}$. Pb–O interactions cause the formation of ribbons along [010] (Fig. 13, bottom).[10] As the H atoms could not be located from difference Fourier maps, they were artificially placed on the O atoms, thus forming [OH]$^-$ anions. The location of the H atoms is directly on the aforementioned mirror plane and thus fully occupied. The distance was constrained to 1.09 Å. Further investigations into the exact H atom location are described in the following sections.

The lead cation is surrounded in the form of a bicapped trigonal prism. The total coordination number of the lead atom is then CN$_{Pb}$ = 6 + 1 + 1. The trigonal prismatic coordination sphere is constructed from four Se ($d_{(Pb–Se)}$ = 3.3174(6), 3.5396(6) Å) and

two O atoms ($d_{(Pb-O)}$ = 2.455(3) Å) with *Se,Se,O*-basal planes (CN "6"). Both side planes built of two Se and two O atoms are capped. The one plane is capped by an N terminus of a [SeCN]⁻ anion ($d_{(Pb-N)}$ = 2.708(7) Å, Fig. 14, left). The other plane is capped by an O atom of the hydroxy group (CN "+1 + 1", $d_{(Pb-O)}$ = 2.360(5) Å). The polyhedra are connected to each other by common *Se,Se,O*-basal planes forming rods along [010]. Along [001], the rods are connected to each other by Pb–O interactions and, as a result, common *O,O*-edges form "double-chains" (Fig. 14, right). *Via* the N terminus, connected [SeCN]⁻ anions are collinear with the Pb–N bond.

The double-chains share common *Se*-vertices with neighbouring double-chains and almost linear [SeCN]⁻ anions (∡$_{Se-C-N}$ = 177.9(5)°, Fig. 15).

Phase purity was checked with PXRD and Rietveld refinement corroborated the model within close error margins (Fig. 16 and Table S3†).

Previous studies have shown that depending on the hydrogen isotope, the Raman shift of the OH antisymmetric vibration ν_{as} can be found in different regions. For the ¹H isotope, the signals are expected in the region of 3600 cm⁻¹, and for the deuterated variant in the region of 2700 cm⁻¹.[51] In the Raman spectrum of Pb[SeCN][OH], the OH-stretch vibration ν_{as} can be found at 3529 cm⁻¹ (see Fig. 17, black plot). To verify the affiliation of this vibration to Pb[SeCN][OH] and exclude the influence of air moisture on the Raman spectrum, a deuterated compound Pb[SeCN][OD] was synthesised. As expected, the OD-stretch vibration ν_{as} was found at 2605 cm⁻¹ (Fig. 17, red plot).

Thermal analysis

To study the thermal behaviour of the compounds in the series Pb[ChCN]₂ (Ch = O, S, Se), we conducted differential scanning calorimetry coupled with thermogravimetry. According to the DSC-TGA data, the compounds Pb[ChCN]₂ decompose upon heating without melting. Also, there is no relationship between the type of chalcogen atom and the respective decomposition temperature.

For Pb[OCN]₂ the onset point of decomposition is at 155 °C, as observed from the thermogravimetric data shown as the black line in Fig. 18. The decomposition is not concomi-
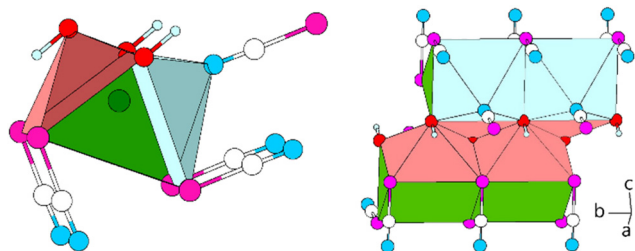

Fig. 15 View along [010] of Pb[SeCN][OH]: double-chains of coordination polyhedra around Pb connected *via* common *Se*-vertices and [SeCN]⁻ anions. Green: Pb, white: C, blue: N, magenta: Se, red: O, light blue: H.

Fig. 16 Rietveld refinement of Pb[SeCN][OH] at 298 K. Black crosses display measured data; the red line represents the refined model, green bars indicate Bragg positions and the grey line displays the difference plot. Further data are compiled in Table S3.†

Fig. 17 Collected Raman spectra of Pb[SeCN][OH] (black) and Pb[SeCN][OD] (red) at 298 K and λ = 633 nm.

Fig. 14 Excerpts from the crystal structure of Pb[SeCN][OH]. Left: coordination polyhedron around Pb (green) in the form of a distorted bicapped tetragonal antiprism, consisting of four Se, three O and one N atom. Right: double-chain of polyhedra stacked along [010]. Green: Pb, white: C, blue: N, magenta: Se, red: O, light blue: H.
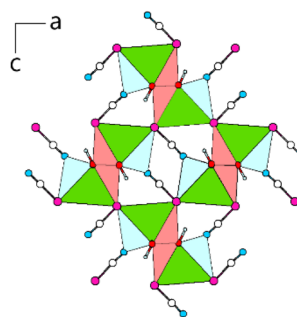
tant with a signal in the DSC thermogram, indicating a very low thermal signature. In the accompanying high-temperature PXRD pattern, reflexes of Pb[OCN]₂ were observed until 210 °C (red, I). In the region between 215 and 440 °C either no unit cell could be indexed or no crystalline compounds were detected (yellow–light blue, II–V). At 445 °C, an orthorhombic

Fig. 18 DSC-TGA analysis of Pb[OCN]₂; black line: TGA graph, red line: DSC graph. Coloured highlights indicate phases observed by high-temperature PXRD.

modification of PbO in the space group *Cmme* (No. 65) was found (blue, VI). After heating up to 540 °C, a tetragonal phase of PbO in the space group *P4/mmm* (No. 129) was found (violet, VII) up to a temperature of 650 °C.[52] Above that, no crystalline phase was observed.

In contrast, Pb[SCN]₂ shows a higher thermal stability up to 284 °C, which is the onset of the decomposition (Fig. 19). Here, the decomposition is concomitant with an exothermic signal in the DSC thermogram at 326 °C. The second step of the decomposition occurs at 700 °C.

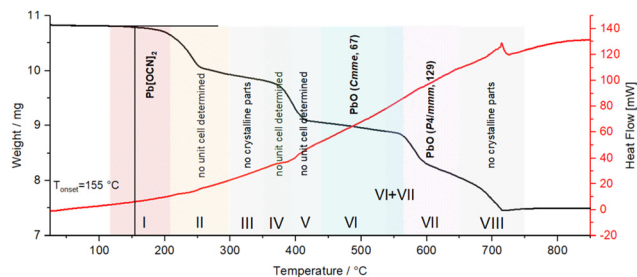Pb[SeCN]₂ shows thermal stability up to 180 °C (see Fig. 20, red, I). In the region between 185 and 215 °C a mixed phase of Pb[SeCN]₂ and PbSe[53] could be detected (see Fig. 20, violet, II). After heating up to 220 °C pure cubic PbSe (No. 225) was found (see Fig. 20, blue, III).[53]
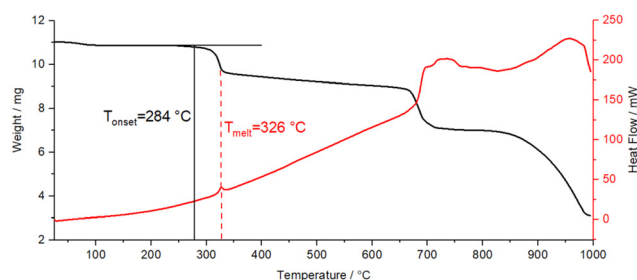

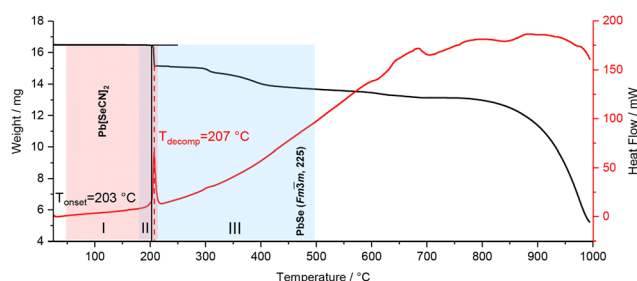**Fig. 19** DSC-TGA analysis of Pb[SCN]₂; black line: TGA graph, red line: DSC graph.

Fig. 20 DSC-TGA analysis of Pb[SeCN]₂; black line: TGA graph, red line: DSC graph. Coloured highlights indicate phases observed by high-temperature PXRD.

Structure and electronic properties

The computed crystal structure parameters of the lead-based compounds under study are reported in Table 1. The agreement between the (B3LYP) calculated and experimentally measured lattice parameters is very good, with the largest deviation of about 3% obtained for the **b** lattice vector of Pb[OCN]₂. Similar results (not explicitly shown) are found when using the PBE0 exchange-correlation functional, confirming the suitability of global hybrid functionals to describe the geometrical features of the lead-based compounds presented here.

The calculated electronic band structures along high-symmetry paths in the Brillouin zone are shown in Fig. 21. All four compounds are wide-bandgap insulators with an electronic band gap of more than 3.8 eV, absorbing only in the high-frequency region of the visible spectrum. Overall, the bands show little dispersion with indirect band gaps for all compounds apart from Pb[SeCN][OH], which is a direct gap material.

To determine the experimental indirect band gap for Pb[ChCN]₂ (Ch = O, S, Se) and the direct band gap for Pb[SeCN][OH], UV-Vis spectra in the range between 200 and 800 nm (~1.5–6.2 eV) were recorded (Fig. S6†). Experimental results fit the calculated trend, where Pb[OCN]₂ has the largest value for the band gap, and Pb[SCN]₂ and Pb[SeCN]₂ are in the same region and show a smaller band gap. The value for the band gap of Pb[SeCN][OH] lies between the values for Pb[OCN]₂ and Pb[ChCN]₂ (Ch = S, Se), which also matches the calculated results.

Analysis of the electronic densities of states (DOS) reveals that the top of the valence band of lead(ɪɪ) selenocyanate and lead(ɪɪ) selenocyanate hydroxide consists predominantly of Se 4p states with additional minor O 2p and N 2p states in Pb[SeCN][OH]. The bottom of the conduction band originates mainly from Pb 6p states. In Pb[OCN]₂, the valence band is a

Table 1 Structural properties of the lead-based compounds under scrutiny, where the experimental and calculated values are listed, together with the relative error of the computed values (with respect to the experimentally measured values) and electronic Kohn–Sham band gap values. DFT values are reported for the B3LYP functional

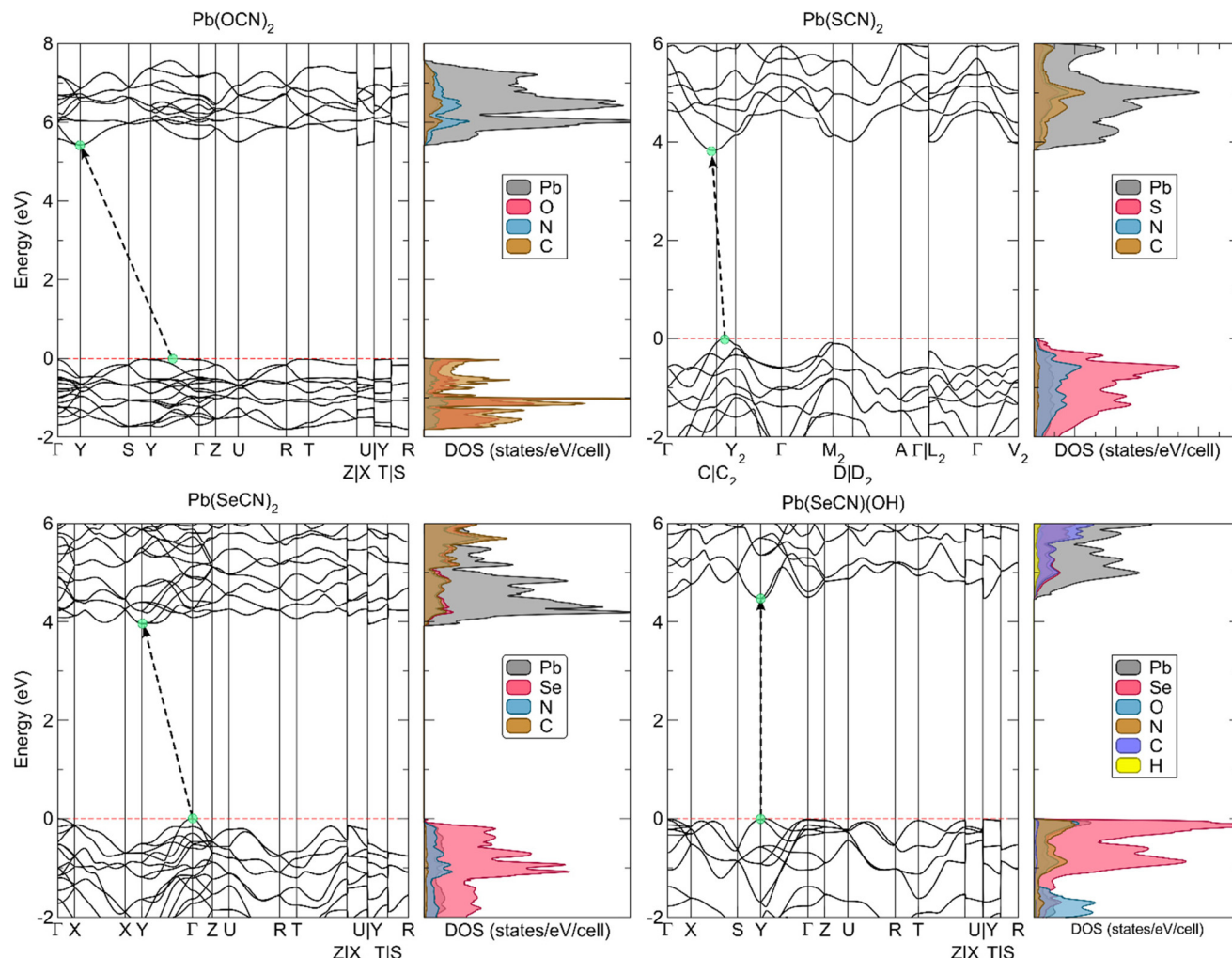| Compound	Space group	a (Å)	b (Å)	c (Å)		E_g (eV)
Pb[OCN]₂	*Pnma* (No. 62)	8.569	3.941	11.660	Exp	
		8.625	4.068	11.820	DFT	5.43 (i)
		0.7	3.2	1.4	Δ (%)	
Pb[SCN]₂	*C2/c* (No. 15)	9.656	6.539	8.251	Exp	
		9.670	6.577	8.096	DFT	3.82 (i)
		0.1	0.6	−1.9	Δ (%)	
Pb[SeCN]₂	*Pnma* (No. 62)	12.479	4.228	10.652	Exp	
		12.555	4.235	10.777	DFT	3.96 (i)
		0.6	0.2	1.2	Δ (%)	
Pb[SeCN][OH]	*Pnma* (No. 62)	8.624	4.167	11.541	Exp	
		8.502	4.184	11.555	DFT	4.47 (d)
		−1.4	0.4	0.1	Δ (%)	

Fig. 21 Electronic band structure together with atomic-projected electronic densities of states of the lead-based compounds under scrutiny. The black dashed arrows and teal circles indicate the fundamental band transition, while the red dashed line indicates the highest occupied crystalline orbital.

mixture of C 2p, N 2p, and O 2p electronic states and the conduction band is derived from Pb 6p states, while in $Pb[SCN]_2$ the valence band consists of a large portion of S 3p states mixed with smaller amounts of N 2p states.

Vibrational spectroscopy

The orthorhombic crystallographic cells of lead(ɪɪ) selenocyanate and lead(ɪɪ) cyanate contain 28 atoms in the unit cell (7 non-equivalent positions); its 84 vibrational modes can be further classified according to the irreducible representation of the *mmm* point group as follows:

$$\Gamma_{\text{total}} = 7 \cdot (2A_g \otimes 1A_u \otimes 1B_{1g} \otimes 2B_{1u} \otimes 2B_{2g} \otimes 1B_{2u} \otimes 1B_{3g} \otimes 2B_{3u}).$$

B_{1u}, B_{2u}, and B_{3u} are IR active modes; A_g, B_{1g}, B_{2g}, and B_{3g} are Raman active, while A_u is silent. For lead(ɪɪ) selenocyanate hydroxide, the irreducible representation is the same, but given that it contains 24 atoms in the unit cell (6 non-equi-

valent positions), the total number of vibrational modes is reduced from 84 to 72.

The monoclinic cell of lead(ɪɪ) thiocyanate contains 14 atoms in the unit cell (4 non-equivalent positions, unique axis *b*), whose 42 vibrational modes are classified according to the irreducible representation of the $2/m$ point group as follows:

$$\Gamma_{\text{total}} = 10A_g \otimes 10A_u \otimes 11B_g \otimes 11B_u.$$

A_u and B_u are IR active and A_g and B_g are Raman active.

Raman spectra calculated under the harmonic approximation are shown in Fig. 22, while the computed frequencies of the Raman active modes in the lead-based compounds studied in this work are reported in Tables S1 and S2.†

Resolving H occupation in Pb[SeCN][OH]

In several of the experimentally measured Raman spectra of Pb[SeCN][OH], a strong vibrational signal around 3000 cm^{-1} was noticed. Given that lead(ɪɪ) selenocyanate hydroxide crys-
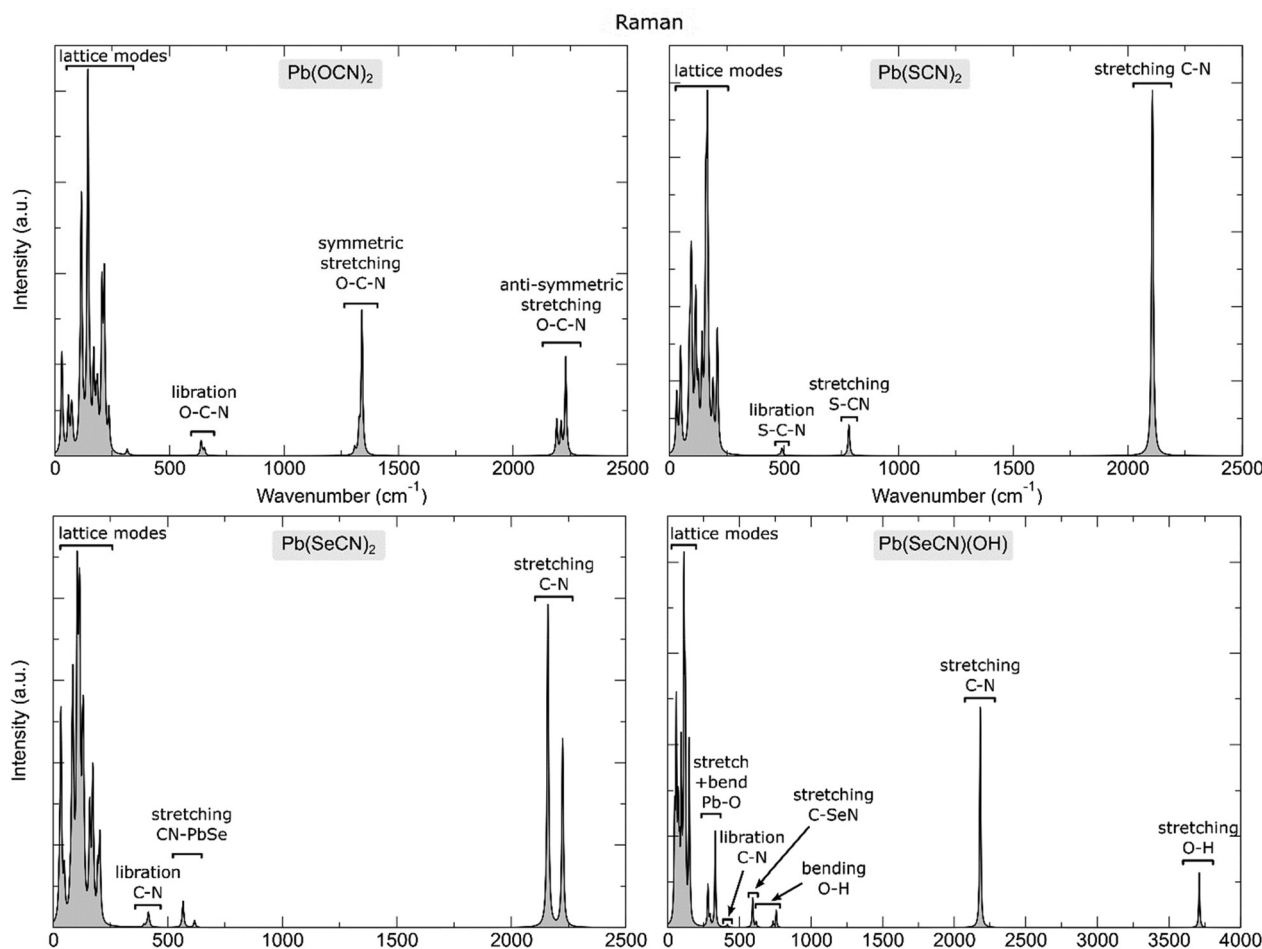
Fig. 22 Calculated Raman spectrum of the lead-based compounds under analysis together with an assignment of the most prominent vibrational features.

tallizes in an orthorhombic crystal system with the space group *Pnma* and that the electron density of the hydrogen atom is difficult to locate exactly for the OH group, the proton was assigned a special position on the *b*-axis, which is a sensible choice for such systems. However, we decided to verify this suggestion using DFT to understand the possible origin of the vibrational frequency around 3000 cm^{-1} and rule out potential inaccuracies from the assignment of the initial H position. Several options were checked: optimization in the *P*1 space group, the displacement of the H atom out of the *ac*-plane, split-site position (50% occupancy of H sites), OH direction alteration, anharmonicity of the OH bond vibration, and overtone mode frequencies (Fig. 23).

In the first scenario, a full geometry optimization without imposing any symmetry on the system did not result in any significant geometry alterations compared to the starting structure with full symmetry relaxation. In the second scenario, H was displaced out of the *ac*-plane where it occupied a special position as a result of the *Pnma* space group. By doing so, the number of symmetry operators of the system was reduced and depending on the motif occupied by the final displaced configurations, different sub-space groups were obtained, as listed

in Table 2. However, upon relaxation (even while strictly imposing the new space groups), the H atoms reverted fully to their position along the *b*-axis, effectively again forming the original *Pnma* space group symmetry.

In the third assessed scenario, a supercell was created where, as a result, only half of hydrogen sites were occupied. This induces a strong cell distortion, with the *a* lattice parameter contracting by 12% and the *c* lattice parameter expanding by more than 14%. This leads, in the vibrational spectrum, to an increase in the intensity of the lattice vibrations, together with a pronounced peak splitting of the pristine C–N symmetric stretching as a result of the symmetry reduction. However, no vibrations were observed between 2200 cm^{-1} and 3500 cm^{-1}, neither in the IR nor Raman spectrum. Also, the intensity of the calculated Raman vibrations had decreased significantly.

The fourth explored scenario included the creation of a supercell where we altered 50% of the OH bond directions along the *b*-axis in such a way that they point towards each other in contrast to the pristine structure, where they always point away from each other. As such, the symmetry is almost entirely reduced, with a residual space group of *P*2$_1$/*m* (No. 11).
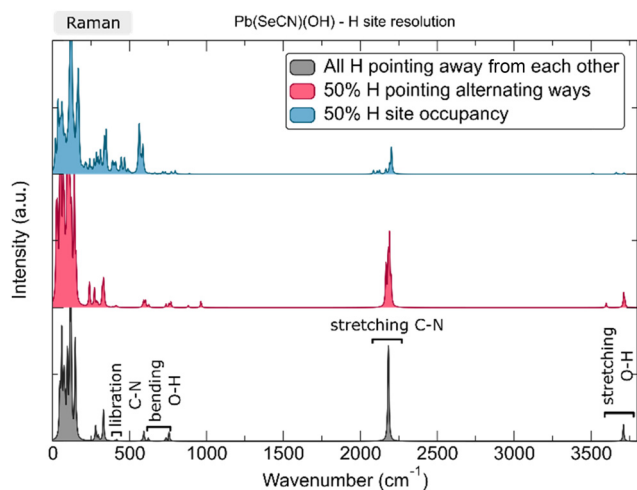
Fig. 23 Calculated Raman spectrum of Pb[SeCN][OH] with varying H-site occupation.

Table 2 Symmetry reduction for Pb[SeCN][OH] systems where the H atoms are displaced out of the *ac*-plane. The sub-space group is listed, together with the initial and final displacement angles with respect to the *ac*-plane. Displacement value of 0.5 in direct coordinates (approx. 0.62 Å in Cartesian coordinates)

H position displacement permutation	Space group	Starting angle wrt to *ac*-plane	Final angle wrt to *ac*-plane
Original	62	0.0°	0.0°
All +b (or −b)	33	45.3°	0.1°
+b −b +b −b	14	45.3°	0.0°
+b −b −b +b	19	45.3°	0.1°
+b +b −b −b	14	45.3°	0.0°

Upon full geometric and atomic relaxation, the structure alters very little, up to a maximum of 2% expansion in the *b* crystallographic direction. The calculated Raman spectrum is displayed in the middle of Fig. 23. In this structure the O–H stretching mode splits due to the lifted degeneracy and displays two distinct peaks split by more than Δ = 100 cm^{-1}. A second possibility was tested as well, with half of the OH bonds pointing in a direction perpendicular to the original OH bond along the *b*-axis, this time with the residual *Pm* space group (No. 6), but

that structure reverted quickly to the starting configuration upon full relaxation.

In the fifth scenario, the anharmonicity of the O–H stretching vibration was considered in the original *Pnma* space group of Pb[SeCN][OH]. The computed frequencies of both IR and Raman active vibrational modes using the VSCF and VCI approaches to treat anharmonicity are listed in Table 3.

For comparison, using the approach of solving the 1D Schrödinger equation yields a harmonic frequency of 3739 cm^{-1} and the fundamental anharmonic frequency of 3552 cm^{-1} (mode no. 69), *i.e.*, significantly different from the frequencies computed using the VSCF and VCI approaches. This illustrates once more the shortcomings of neglecting explicit phonon–phonon coupling, which can be effectively and efficiently treated in the VSCF and VCI approaches implemented in CRYSTAL. First, anharmonic treatment of the O–H stretch was performed as a single-mode, labelled as "intrinsic anharmonic" in Table 3, where mode–mode coupling is fully neglected. There, VSCF and VCI are formally identical.[44] In the second approach, we allowed all the stretching modes to couple with each other (8 modes in total). The results of these analyses indicate that anharmonic shifts in frequency in Pb[SeCN][OH] are no larger than 90 cm^{-1}, which is observed for the A$_g$ Raman active O–H stretch.

In the final scenario, the possibility that the measured spectra display overtone features is assessed. First overtones were computed for the initial lead(ɪɪ) selenocyanate hydroxide and the results indicated 16 potential combinations between the O–H bending and C–N stretching modes, which produce frequencies between 2909 cm^{-1} and 2941 cm^{-1}. In addition, we computed the overtones for the Pb[SeCN][OH] structure with the OH bonds pointing in opposite directions (scenario four), and there we identified 80 potential combinations of modes that produce frequencies between 2903 cm^{-1} and 3164 cm^{-1}.

Given the difficulty in detecting experimentally the exact H positions in the lattice as well as their potential to occupy sites that vary in direction across an experimentally synthesized sample, it is most likely that the measured vibrational frequencies noted in the area of around 3000 cm^{-1} originate from an overtone of the fundamental O–H bending and C–N stretching modes.

Table 3 Fundamental O–H stretching frequencies (in cm^{-1}) of Pb(SeCN)(OH) as computed within the harmonic approximation and by taking into account anharmonicity at different levels of approximation. VSCF – vibrational self-consistent field; VCI – vibrational configuration interaction

Mode #	Symmetry label	Harmonic	Intrinsic anharmonic	VSCF (8 modes)	VCI@VSCF (8 modes)
65	B$_{1u}$	2174	2180	2174	2171
66	A$_g$	2181	2176	2181	2170
67	B$_{2u}$	2184	2190	2184	2181
68	B$_{3g}$	2184	2190	2184	2181
69	A$_g$	3712	3678	3699	3624
70	B$_{1u}$	3712	3762	3685	3674
71	B$_{3g}$	3713	3761	3686	3675
72	B$_{2u}$	3713	3762	3686	3675

Conclusions

In this work, we have described the synthesis of the Pb[ChCN]$_2$ series of compounds with Ch = O, S, Se, and Pb[SeCN][OH]. Whereas the lead thiocyanate[54] and selenocyanate compounds are able to form hydroxides Pb[ChCN][OH] with Ch = S, Se under neutral conditions, the cyanate homologue solely forms Pb[OCN]$_2$.[10] All compounds were characterized by single-crystal and powder X-ray diffraction, Raman spectroscopy, solid-state DFT analysis, and thermogravimetric analysis/differential scanning calorimetry. For Pb[SeCN][OH], no H atoms could be found by X-ray diffraction and, for the structure refinements, the H atom positions were restrained in accordance with the symmetry of the chosen space group. For verification of the presence of the hydroxy group, Raman spectroscopy was performed. Additionally, a deuterated homologue was synthesized and characterized by Raman spectroscopy and powder X-ray diffraction. In the Raman spectra, the corresponding signals were observed and assigned to the calculated vibrations as well as compared with the literature data. Thermal decomposition of Pb[ChCN]$_2$ (Ch = O, S, Se) was followed by DSC/TGA analysis for Ch = O, S, Se, and high-temperature powder diffraction for Ch = O, Se. Pb[SCN]$_2$ shows the highest thermal stability in the series up to 284 °C. Crystalline Pb[OCN]$_2$ and Pb[SeCN]$_2$ were found by heating up to ~200 °C in ht-PXRD. For all four of the compounds studied, DFT calculations were performed. According to the DFT studies, all four compounds are wide-bandgap insulators with electronic band gaps exceeding 3.8 eV, absorbing only in the high-frequency region of the visible spectrum. Overall, the bands show minimal dispersion with indirect band gaps for all compounds except for Pb[SeCN][OH], which is identified as a direct-gap material. For Pb[SeCN][OH], resolving the occupation of the H atoms was performed following several scenarios, although none could predict the accurate position of the H atoms. Based on the calculated Raman vibrations and their comparison with collected data, it is suggested that the location of the H atoms is directly on the aforementioned mirror plane and thus fully in accordance with the space group symmetry.

Author contributions

FT conceptualized and led the study. AS performed the experiments and led the analytical investigations. AŽ and NHdL were responsible for the computational work. The manuscript was written through contributions from all authors. All authors have given approval for the final version of the manuscript.

Data availability

Crystallographic data for Pb[OCN]$_2$, Pb[SCN]$_2$, Pb[SeCN]$_2$ and Pb[SeCN][OH] have been deposited at the CCDC under deposition numbers 2383820, 2383821, 2383822 and 2383823.

Additional data supporting this article have been included as part of the ESI.†

Conflicts of interest

There are no conflicts to declare.

Acknowledgements

References

1 A. Shlyaykher, M. Ehmann, A. J. Karttunen and F. Tambornino, A Comprehensive Study on the Full Series of Alkali–Metal Selenocyanates AI[SeCN] (AI=Li–Cs), *Eur. J. Chem.*, 2021, **27**, 13552–13557.

2 J. Liebig and F. Wöhler, Untersuchungen über die Cyansäure, *Annu. Phys. Chem.*, 1830, **28**, 188–191.

3 A. C. Cumming, CXXXV.—The formation of urea by the direct hydrolysis of lead cyanate, *J. Chem. Soc., Trans.*, 1903, **83**, 1391–1394.

4 C. W. Blomstrand, Zur Kenntniss der gepaarten Verbindungen des fünfatomigen Stickstoffs, *J. Prakt. Chem.*, 1871, **2**, 201.

5 J. L. Gay-Lussac, Untersuchungen über die Blausäure, *Ann. Phys.*, 1815, 139–168.

6 F. Wöhler, Bildung der Cyansäure auf neuem Wege, und fernere Untersuchungen über die Cyansäure und deren Salze, *Gilbert's Ann.*, 1823, **73**, 157.

7 J. Liebig, Über einige Produkte, welche durch die Zersetzung mehrerer Salze vermittelst Chlor erhalten werden, *Ann. Phys. Chem.*, 1829, **1**, 541–572.

8 H. E. Williams, *Cyanogen Compounds Their Chemistry, Detection and Estimation*, Edward Arnold & Co., London, 2nd edn, 1948.

9 J. A. A. Mokuolu and J. C. Speakman, The crystal structure of lead thiocyanate, *Chem. Commun.*, 1966, 25.

10 V. Adovasio and M. Nardelli, Metal–Hydroxy Ribbons in Pb(OH)(NCS), *Acta Crystallogr., Sect. C: Cryst. Struct. Commun.*, 1995, **51**, 380–382.

11 J. G. Labram, N. R. Venkatesan, C. J. Takacs, H. A. Evans, E. E. Perry, F. Wudl and M. L. Chabinyc, Charge transport in a two-dimensional hybrid metal halide thiocyanate compound, *J. Mater. Chem. C*, 2017, **5**, 5930–5938.

12 Q. Jiang, D. Rebollar, J. Gong, E. L. Piacentino, C. Zheng and T. Xu, Pseudohalide–Induced Moisture Tolerance in

Perovskite $CH_3NH_3Pb(SCN)_2I$ Thin Films, *Angew. Chem., Int. Ed.*, 2015, **54**, 7617–7620.

13 W. Ke, C. Xiao, C. Wang, B. Saparov, H. S. Duan, D. Zhao, Z. Xiao, P. Schulz, S. P. Harvey, W. Liao, W. Meng, Y. Yu, A. J. Cimaroli, C. S. Jiang, K. Zhu, M. Al-Jassim, G. Fang, D. B. Mitzi and Y. Yan, Employing Lead Thiocyanate Additive to Reduce the Hysteresis and Boost the Fill Factor of Planar Perovskite Solar Cells, *Adv. Mater.*, 2016, **28**, 5214–5221.

14 B. A. Koscher, J. K. Swabeck, N. D. Bronstein and A. P. Alivisatos, Essentially Trap-Free $CsPbBr_3$ Colloidal Nanocrystals by Postsynthetic Thiocyanate Surface Treatment, *J. Am. Chem. Soc.*, 2017, **139**, 6566–6569.

15 B. Walker, G. Kim and J. Y. Kim, Pseudohalides in Lead–Based Perovskite Semiconductors, *Adv. Mater.*, 2019, **31**, 1807029–1807029.

16 W. Crookes, Ueber die Selencyanide, *Ann. Chem. Pharm.*, 1851, **78**, 177–187.

17 G. Brauer, *Handbuch der Präparativen Anorganischen Chemie*, Ferdinand Enke Verlag, Stuttgart, 3. Auflage, 1975.

18 *X-Area 1.88*, Stoe & Cie GmbH, Darmstadt, Germany, 2019.

19 G. M. Sheldrick, A short history of Shelx, *Acta Crystallogr., Sect. F: Struct. Biol. Cryst. Commun.*, 2008, **64**, 112–122.

20 O. V. Dolomanov, L. J. Bourhis, R. J. Gildea, J. A. K. Howard and H. Puschmann, OLEX2: A complete structure solution, refinement and analysis program, *J. Appl. Crystallogr.*, 2009, **42**, 339–341.

21 K. Brandenburg and H. Putz, *DIAMOND, Program for X-Ray Strkucture Analysis*, Crystal Impact GbR, Bonn, Gemany, 2005.

22 H. M. Rietveld, A profile refinement method for nuclear and magnetic structures, *J. Appl. Crystallogr.*, 1969, **2**, 65–71.

23 A. A. Coelho, TOPAS and TOPAS-Academic : an optimization program integrating computer algebra and crystallographic objects written in C++, *J. Appl. Crystallogr.*, 2018, **51**, 210–218.

24 R. Dovesi, A. Erba, R. Orlando, C. M. Zicovich-Wilson, B. Civalleri, L. Maschio, M. Rérat, S. Casassa, J. Baima, S. Salustro and B. Kirtman, Quantum-mechanical condensed matter simulations with CRYSTAL, *Wiley Interdiscip. Rev.: Comput. Mol. Sci.*, 2018, **8**, e1360.

25 F. Pascale, C. M. Zicovich-Wilson, F. López Gejo, B. Civalleri, R. Orlando and R. Dovesi, The calculation of the vibrational frequencies of crystalline compounds and its implementation in the CRYSTAL code, *J. Comput. Chem.*, 2004, **25**, 888–897.

26 C. M. Zicovich-Wilson, F. Pascale, C. Roetti, V. R. Saunders, R. Orlando and R. Dovesi, Calculation of the vibration frequencies of α-quartz: The effect of Hamiltonian and basis set, *J. Comput. Chem.*, 2004, **25**, 1873–1881.

27 A. Erba, J. K. Desmarais, S. Casassa, B. Civalleri, L. Donà, I. J. Bush, B. Searle, L. Maschio, L. Edith-Daga, A. Cossard, C. Ribaldone, E. Ascrizzi, N. L. Marana, J.-P. Flament and B. Kirtman, CRYSTAL23: A Program for Computational Solid State Physics and Chemistry, *J. Chem. Theory Comput.*, 2022, **19**, 6891–6932, DOI: **10.1021/acs.jctc.2c00958**.

28 A. D. Becke, A new mixing of Hartree–Fock and local density–functional theories, *J. Chem. Phys.*, 1993, **98**, 1372–1377.

29 C. Lee, W. Yang and R. G. Parr, Development of the Colle-Salvetti correlation-energy formula into a functional of the electron density, *Phys. Rev. B: Condens. Matter Mater. Phys.*, 1988, **37**, 785–789.

30 D. Vilela Oliveira, J. Laun, M. F. Peintinger and T. Bredow, BSSE-correction scheme for consistent gaussian basis sets of double- and triple-zeta valence with polarization quality for solid-state calculations, *J. Comput. Chem.*, 2019, **40**, 2364–2376.

31 C. Pisani, R. Dovesi and C. Roetti, *Hartree-Fock Ab Initio Treatment of Crystalline Systems*, Springer Berlin Heidelberg, Berlin, Heidelberg, 1988, vol. 48.

32 R. Dovesi, V. R. Saunders, C. Roetti, R. Orlando, C. M. Zicovich-Wilson, F. Pascale, B. Civalleri, K. Doll, N. M. Harrison, I. J. Bush, P. D'Arco, M. Llunell, M. Causà, Y. Noël, L. Maschio, A. Erba, M. Rerat and S. Casassa, *Crystal17 User's Manual* 2017.

33 H. J. Monkhorst and J. D. Pack, Special points for Brillouin-zone integrations, *Phys. Rev. B: Solid State*, 1976, **13**, 5188–5192.

34 S. Grimme, J. Antony, S. Ehrlich and H. Krieg, A consistent and accurate ab initio parametrization of density functional dispersion correction (DFT-D) for the 94 elements H-Pu, *J. Chem. Phys.*, 2010, **132**, 1–19.

35 S. Grimme, S. Ehrlich and L. Goerigk, Effect of the damping function in dispersion corrected density functional theory, *J. Comput. Chem.*, 2011, **32**, 1456–1465.

36 S. Grimme, A. Hansen, J. G. Brandenburg and C. Bannwarth, Dispersion-Corrected Mean-Field Electronic Structure Methods, *Chem. Rev.*, 2016, **116**, 5105–5154.

37 Y. Hinuma, G. Pizzi, Y. Kumagai, F. Oba and I. Tanaka, Band structure diagram paths based on crystallography, *Comput. Mater. Sci.*, 2017, **128**, 140–184.

38 L. Maschio, B. Kirtman, M. Rérat, R. Orlando and R. Dovesi, Ab initio analytical Raman intensities for periodic systems through a coupled perturbed Hartree-Fock/Kohn-Sham method in an atomic orbital basis. II. Validation and comparison with experiments, *J. Chem. Phys.*, 2013, **139**, 1–13.

39 L. Maschio, B. Kirtman, R. Orlando and M. Rèrat, Ab initio analytical infrared intensities for periodic systems through a coupled perturbed Hartree-Fock/Kohn-Sham method, *J. Chem. Phys.*, 2012, **137**, 204113.

40 F. Pascale, S. Tosoni, C. Zicovich-Wilson, P. Ugliengo, R. Orlando and R. Dovesi, Vibrational spectrum of brucite, $Mg(OH)_2$: a periodic ab initio quantum mechanical calculation including OH anharmonicity, *Chem. Phys. Lett.*, 2004, **396**, 308–315.

41 P. Ugliengo, F. Pascale, M. Mérawa, P. Labéguerie, S. Tosoni and R. Dovesi, Infrared Spectra of Hydrogen-Bonded Ionic Crystals: Ab Initio Study of $Mg(OH)_2$ and β-$Be(OH)_2$, *J. Phys. Chem. B*, 2004, **108**, 13632–13637.

42 A. Erba, J. Maul, M. Ferrabone, R. Dovesi, M. Rérat and P. Carbonnière, Anharmonic Vibrational States of Solids from DFT Calculations. Part II: Implementation of the VSCF and VCI Methods, *J. Chem. Theory Comput.*, 2019, **15**, 3766–3777.

43 A. Erba, J. Maul, M. Ferrabone, P. Carbonnière, M. Rérat and R. Dovesi, Anharmonic Vibrational States of Solids from DFT Calculations. Part I: Description of the Potential Energy Surface, *J. Chem. Theory Comput.*, 2019, **15**, 3755–3765.

44 R. G. Schireman, J. Maul, A. Erba and M. T. Ruggiero, Anharmonic Coupling of Stretching Vibrations in Ice: A Periodic VSCF and VCI Description, *J. Chem. Theory Comput.*, 2022, **18**, 4428–4437.

45 D. Mitoli, J. Maul and A. Erba, Anharmonic Terms of the Potential Energy Surface: A Group Theoretical Approach, *Cryst. Growth Des.*, 2023, **23**, 3671–3680, DOI: **10.1021/acs.cgd.3c00104**.

46 *Origin(Pro), Version 8G.* OriginLab Corporation, Northampton, MA, USA., 2008.

47 J. A. A. Mokuolu and J. C. Speakman, The crystal structure of lead(II) thiocyanate, *Acta Crystallogr., Sect. B: Struct. Crystallogr. Cryst. Chem.*, 1975, **31**, 172–176.

48 L. Link and R. Niewa, Polynator : a tool to identify and quantitatively evaluate polyhedra and other shapes in crystal structures, *J. Appl. Crystallogr.*, 2023, **56**, 1855–1864, DOI: **10.1107/S1600576723008476**.

49 H. Zabrodsky, S. Peleg and D. Avnir, Continuous Symmetry Measures, *J. Am. Chem. Soc.*, 1992, **114**, 7843–7851.

50 R. D. Shannon, Revised effective ionic radii and systematic studies of interatomic distances in halides and chalcogenides, *Acta Crystallogr., Sect. A: Cryst. Phys., Diffr., Theor. Gen. Crystallogr.*, 1976, **32**, 751–767.

51 A. Zarei, S. Klumbach and H. Keppler, The Relative Raman Scattering Cross Sections of H_2O and D_2O, with Implications for In Situ Studies of Isotope Fractionation, *CS Earth Space Chem.*, 2018, **2**, 925–934.

52 P. Boher, P. Garnier, J. R. Gavarri and A. W. Hewat, Monoxyde quadratique PbOα(I): Description de la transition structurale ferroélastique, *J. Solid State Chem.*, 1985, **57**, 343–350.

53 Y. Noda, K. Masumoto, S. Ohba, Y. Saito, K. Toriumi, Y. Iwata and I. Shibuya, Temperature dependence of atomic thermal parameters of lead chalcogenides, PbS, PbSe and PbTe, *Acta Crystallogr., Sect. A: Found. Crystallogr.*, 1987, **43**, 1443–1445.

54 B. Akteries and J. C. Jochims, Reactions of carbonyl diisocyanate with amides and acids, *Chem. Ber.*, 1986, **119**, 669–682.